Available online at www.sciencedirect.com
SCIENCE DIRECT®
Journal of Magnetic Resonance 177 (2005) 247–260
JMR Journal of Magnetic Resonance
www.elsevier.com/locate/jmr

Effects of finite pulse width on two-dimensional Fourier transform electron spin resonance

Zhichun Liang, Richard H. Crepeau, Jack H. Freed *

Baker Laboratory of Chemistry and Chemical Biology Cornell University, Ithaca, NY 14853-1301, USA

Received 3 June 2005; revised 14 July 2005
Available online 16 September 2005

Abstract

Two-dimensional (2D) Fourier transform ESR techniques, such as 2D-ELDOR, have considerably improved the resolution of ESR in studies of molecular dynamics in complex fluids such as liquid crystals and membrane vesicles and in spin labeled polymers and peptides. A well-developed theory based on the stochastic Liouville equation (SLE) has been successfully employed to analyze these experiments. However, one fundamental assumption has been utilized to simplify the complex analysis, viz. the pulses have been treated as ideal non-selective ones, which therefore provide uniform irradiation of the whole spectrum. In actual experiments, the pulses are of finite width causing deviations from the theoretical predictions, a problem that is exacerbated by experiments performed at higher frequencies. In the present paper we provide a method to deal with the full SLE including the explicit role of the molecular dynamics, the spin Hamiltonian and the radiation field during the pulse. The computations are rendered more manageable by utilizing the Trotter formula, which is adapted to handle this SLE in what we call a "Split Super-Operator" method. Examples are given for different motional regimes, which show how 2D-ELDOR spectra are affected by the finite pulse widths. The theory shows good agreement with 2D-ELDOR experiments performed as a function of pulse width.

Keywords: Stochastic Liouville equation; 2D-ELDOR; ESR; Rotational diffusion; Split super-operator; Trotter formula

1. Introduction

The two-dimensional (2D) Fourier transform ESR experiment known as 2D-ELDOR [1–3] is a technique that provides considerable enhancement in resolution to ordering and dynamics as compared to conventional ESR spectroscopy. It has been employed extensively in studies of membrane vesicles using nitroxide-labeled lipids and cholesterol [4–8], spin probes in liquid crystals [9–11], and spin-labeled polymers and peptides [12,13]. The three pulse 2D-ELDOR sequence is shown in Fig. 1.

In 2D-ELDOR, crosspeaks appear that are a measure of magnetization transfer by spin relaxation processes during the mixing time, T_m. The principal relaxation mechanisms are the intramolecular electron–nuclear dipolar (END) interactions, which lead to nuclear spin flip transitions that report on the rate of rotational reorientation, and the Heisenberg exchange (HE) rate which reports on the bimolecular collision rate of the spin-labeled molecules. The pattern of cross-peaks, as well as how they grow in with T_m, enables one to distinguish the contributions from each relaxation mechanism. In the 2D-ELDOR experiment there are two coherence pathways, the S_{c+}, which is FID-like and the S_{c-}, which is echo-like, because it is refocused by the last pulse. As a result, in the presence of inhomogeneous broadening (IB) the S_{c-} spectra are substantially sharper due to the echo-like cancellation of the IB, and are less attenuated by finite dead times. It is possible to distinguish the homogeneous broadening (HB) and the IB because the

* Corresponding author. Fax: +1 607 255 6969.
E-mail address: jhf@ccmr.cornell.edu (J.H. Freed).

1090-7807/$ - see front matter © 2005 Elsevier Inc. All rights reserved.
doi:10.1016/j.jmr.2005.07.024

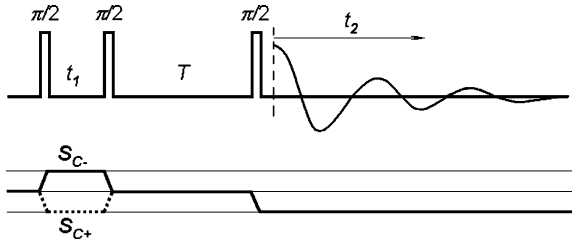

Fig. 1. Pulse sequence and coherence pathways of 2D-ELDOR. The upper, middle, and lower horizontal lines in the latter correspond to coherences of +1, 0, and −1, respectively.

refocusing of IB is achieved along one spectral dimension, whereas it is not refocused along the orthogonal spectral dimension. (This is strictly true after the S_{c-} spectrum is transformed into a SECSY spectrum, [4–8]). This is important, since the IB contains information on the microscopic ordering of the spin labels, whereas the HB reports on the molecular dynamics. Complex fluids are generally characterized by microscopic order but macroscopic disorder (i.e., the MOMD effect). In addition, one may use the different shapes of the autopeaks and cross-peaks to precisely distinguish the contribution to IB from proton shf interactions, which are the same for each hf line, and the effect of MOMD, which varies for each hf line. These are key features of 2D-ELDOR, which yield greatly improved resolution to dynamics and ordering in complex fluids such as membranes.

Lee et al. [14] have provided a detailed theory for 2D-ELDOR and related experiments based upon the stochastic Liouville equation (SLE), that is applicable to complex fluids, and it has been the basis for analysis of these experiments in conjunction with least-squares fitting [15]. Also a more sophisticated version has been introduced to model the complex dynamics in such fluid and disordered systems [10]. However, a key simplifying assumption has remained in the theory, viz., the pulses have been treated as ideal non-selective ones, which have the effect of irradiating the whole spectrum uniformly. In reality, this is never the case, although considerable instrumental progress has been made to achieve very short $\pi/2$ pulses, as short as 3 ns [16], which do provide good coverage even for slow motional ESR spectra at conventional ESR frequencies. Such short pulses are not generally available in either home-built or commercial spectrometers. In the past empirical methods were employed to correct for incomplete coverage [4]. Very recently, with the advent of high frequency (95 GHz) 2D-ELDOR [17], wherein the spectral extent is greatly increased, the need to better understand the effects of using realistic pulses of finite temporal extent becomes even more important. In fact, not only should one consider the effects of the finite pulse on the spectrum, but also the molecular dynamics and relaxation occurring during the time of the pulse.

To address these matters one therefore needs to solve the SLE in the presence (and in the absence) of the finite pulses. It is the purpose of the present paper to address this challenge. The task of dealing with the full SLE including radiation field during the pulse is complicated by the fact that the submatrices of the SLE representing the different orders of coherence (± 1 for the off-diagonal density matrix elements and 0 for the diagonal and pseudo-diagonal density matrix elements as described in [14]) are now coupled by the radiation field and must therefore be calculated as one very large and cumbersome supermatrix. These submatrices are decoupled during the free evolution periods, which is all that is needed to be calculated in the Lee, Budil, and Freed theory (LBF, [14]) that assumed ideal pulses, so these submatrices could be separately diagonalized. This is a great simplification for the LBF theory, but was a key challenge in the present work.

Rather than having to diagonalize the full supermatrix, which can assume huge dimensions with a more complex structure of its elements, we decided to employ an approach similar to the "Split Hamiltonian" method previously used by Salikhov et al. [18] and Saxena and Freed [13] to separate out the effects of the main part of the spin Hamiltonian neglecting the radiation from the radiation term, and then to deal with their combined effect using successive short time steps via the Trotter formula [19,20]. In these previous applications to spin-echo modulation and double-quantum coherence ESR, respectively, the molecular dynamics and spin relaxation were largely ignored, so only the time evolution of the density matrix under the effect of the spin-Hamiltonian was considered.

In the present work, the Trotter formula is applied to the full SLE including the explicit role of the molecular dynamics and microscopic ordering for the duration of the finite pulse. By separating, or splitting out the role of the radiation from the other terms in the SLE we show it is possible to calculate the time evolution during the pulse by just diagonalizing the submatrices for the different orders of coherence using the algorithms that are available from the LBF theory. This "Split Super-Operator" method is shown to be very effective in enabling the analysis of the effects of finite pulses in 2D-ELDOR experiments after we establish subtle but important features of its application to the SLE. Computation times are however significantly increased over those for the LBF theory involving ideal pulses, as one would expect, but the resulting formulation is a tractable and useful one. Although we focus on 2D-ELDOR in this paper, the theory is clearly equally applicable to other 2D-FT ESR techniques such as COSY and SECSY ESR (cf. [12]).

It is hoped that the ability to analyze the effects of finite pulses in 2D-ELDOR will make this important

technique more accessible to other laboratories engaged in pulsed ESR spectroscopy.

In Section 2, we describe the new theory encompassing finite pulses. Then in Section 3, we provide results of the theory examining effects of different pulse widths on 2D-ELDOR spectra at 9 and 95 GHz. In addition, we compare with experiments as a function of pulse width and show the very good agreement achieved.

2. Theory

2.1. Stochastic Liouville equation

Let us first define our model system, which is a spin-labeled molecule (e.g., with a nitroxide). The molecule is undergoing reorientation in an anisotropic medium. In ESR, to study the molecular reorientation dynamics and ordering, the spin-labeled molecule is placed in a static magnetic field, B_0. The two major magnetic interactions in this system are: the Zeeman interaction between B_0 and the electron spin ($S = 1/2$) and the hyperfine interaction between S and the nuclear spin ($I = 1$) in the nitroxide. When the system is subject to a microwave pulse of intensity B_1, there is, in addition, the magnetic interaction between S and B_1.

We consider the 2D-ELDOR experiment on the system defined above, as our prototype. Its pulse sequence and coherence transfer pathways are presented in Fig. 1. The sequence contains three $\pi/2$ pulses followed by three respective time intervals. (The discussion is focused on 2D-ELDOR, since it is the most commonly employed [14]). Other relevant pulse ESR experiments can be treated either as special cases of 2D-ELDOR, e.g., COSY data may be generated by letting the mixing time T_m in Fig. 1 equal zero, or else the same methodology can be built up to include more complex pulse sequences.

The 2D-ELDOR signal in Fig. 1 may be analyzed by following the time evolution of the spin magnetization during the corresponding pulse sequence. In the slow motion ESR theory, such a time evolution is described in terms of the stochastic Liouville equation (SLE) of the spin density operator $\rho(\Omega, t)$ [21,22],

$$\begin{aligned}\frac{\partial}{\partial t}\hat{\rho}(\Omega,t) &= -\mathrm{i}[\hat{\mathscr{H}}(\Omega,t),\hat{\rho}(\Omega,t)] - \hat{\Gamma}(\Omega)[\hat{\rho}(\Omega,t) \\ &\quad - \hat{\rho}_{\mathrm{eq}}(\Omega,t)] \\ &= -\mathrm{i}\hat{\mathscr{H}}^{\times}(\Omega,t)\hat{\rho}(\Omega,t) - \hat{\Gamma}(\Omega)[\hat{\rho}(\Omega,t) \\ &\quad - \hat{\rho}_{\mathrm{eq}}(\Omega,t)]. \end{aligned} \tag{1}$$

Here $\hat{\rho}_{\mathrm{eq}}(\Omega,t)$ is the instantaneous equilibrium density operator:

$$\hat{\rho}_{\mathrm{eq}}(\Omega,t) = P_0(\Omega)\frac{\exp[-h\hat{\mathscr{H}}(\Omega,t)/k_BT]}{Tr\{\exp[-h\hat{\mathscr{H}}(\Omega,t)/k_BT]\}}, \tag{2}$$

where k_B is Boltzmann's constant and T is the absolute temperature. In Eq. (1), the spin dynamics is characterized by the quantum operator $\hat{\mathscr{H}}(\Omega,t)$,

$$\hat{\mathscr{H}}(\Omega,t) = \hat{\mathscr{H}}_0(\Omega) + \hat{\mathscr{H}}_1(t), \tag{3}$$

where the total spin Hamiltonian has been divided into two terms, with $\hat{\mathscr{H}}_0$ representing the contribution due to the free evolution of the spins in the absence of the radiation and $\hat{\mathscr{H}}_1$ being due to the interaction of the electron spin S with the microwave radiation. On the other hand, the molecular reorienting dynamics in Eq. (1) is characterized by the classical stochastic (Markovian) operator $\hat{\Gamma}(\Omega)$, in the equation of motion for the probability distribution function, $P(\Omega,t)$

$$\frac{\partial}{\partial t}P(\Omega,t) = -\hat{\Gamma}(\Omega)P(\Omega,t), \tag{4}$$

where Ω is the molecular orientation.

Depending on the relative strengths of $\hat{\mathscr{H}}_0(\Omega)$, $\hat{\mathscr{H}}_1(t)$, and $\hat{\Gamma}(\Omega)$, Eq. (1) may lead to different types of solutions. In the following sections, we will solve Eq. (1) for a few cases of experimental interest.

2.2. Stochastic Liouville superoperator

We first concentrate on the three time intervals following the three $\pi/2$ pulses. In the absence of the radiation, $\hat{\mathscr{H}}_1(t)$ vanishes. The equilibrium density operator in Eq. (2) becomes, in the high-temperature approximation [21–23]

$$\hat{\rho}_{\mathrm{eq}}(\Omega) = P_0(\Omega)\frac{1}{N}\left[1 - \frac{h\hat{\mathscr{H}}_0(\Omega)}{k_BT}\right], \tag{5}$$

where N is the total number of spin states. The equilibrium orientational distribution, $P_0(\Omega)$, can be expressed in terms of the molecular reorienting potential, $U(\Omega)$ as

$$P_0(\Omega) = \frac{\exp[-U(\Omega)/k_BT]}{\langle\exp[-U(\Omega/k_BT)]\rangle}, \tag{6}$$

where the angular brackets imply an ensemble average. Then, Eq. (1) can be simplified to

$$\frac{\partial}{\partial t}\hat{\chi}(\Omega,t) = -\hat{\mathscr{L}}(\Omega)\hat{\chi}(\Omega,t). \tag{7}$$

Here the stochastic Liouville superoperator, $\hat{\mathscr{L}}(\Omega)$, and the reduced spin density operator, $\hat{\chi}(\Omega,t)$, have been defined as

$$\hat{\mathscr{L}}(\Omega) \equiv i\hat{\mathscr{H}}_0^{\times}(\Omega) + \hat{\Gamma}(\Omega) \tag{8}$$

and

$$\hat{\chi}(\Omega,t) \equiv \hat{\rho}(\Omega,t) - \hat{\rho}_{\mathrm{eq}}(\Omega), \tag{9}$$

respectively, with $\hat{\rho}_{\mathrm{eq}}(\Omega)$ given by Eq. (5). The formal solution to Eq. (7) can easily be obtained

$$\hat{\chi}(\Omega,t+t_0) = \mathrm{e}^{-\hat{\mathscr{L}}(\Omega)t}\hat{\chi}(\Omega,t_0), \tag{10}$$

which can be further expressed in terms of the eigenfunctions, which form the orthogonal matrix, O, and the eigenvalues of $\hat{\mathscr{L}}(\Omega)$ contained in the diagonal matrix, Λ [14]

$$\hat{\chi}(\Omega, t+t_0) = O\mathrm{e}^{-\Lambda t}O^{\mathrm{tr}}\hat{\chi}(\Omega, t_0). \tag{11}$$

It is now helpful to specify the detailed forms for the spin Hamiltonian and diffusion operator. For brevity of presentation, we emphasize the simplest case where the spin-labeled molecule has a cylindrically symmetric shape and is reorienting in an isotropic medium. More general formulations of the SLE for anisotropic probe potential are given elsewhere [24]. Discussion of a cage potential is also given elsewhere [25,26]. The case of anisotropic potential has been incorporated into our finite-pulse computer program, but in this paper, we will illustrate the theory with the simple isotropic case. For the system we have chosen, the spin Hamiltonian takes on the following form:

$$\hat{\mathscr{H}}^{\mathrm{x}}_0 = \sum_{\mu=g,A}\sum_{l=0,2}\sum_{m=-l}^{l}\sum_{m'=-l}^{l}\hat{A}^{(l,m)^{\mathrm{x}}}_{\mu,L}\mathscr{D}^{l}_{mm'}(\mathbf{\Omega}_{LR})F^{(l,m')^{*}}_{\mu,R}, \tag{12}$$

where two reference frames are introduced: the laboratory frame, L, with its z-axis along the static magnetic field and the diffusion frame, R, with the z-axis along the long axis of the cylindrical molecule. The magnetic tensor frame has been taken to coincide with the R frame (again for purposes of simplifying the present discussion). The electron and nuclear tensor components, $\hat{A}^{(l,m)}_{\mu,L}$, and the magnetic tensor components, $F^{(l,m')}_{\mu,R}$, are most conveniently expressed in the L frame and the R frame, respectively. These components have been summarized in [27]. The Wigner rotational matrix, $\mathscr{D}^{l}_{mm'}(\mathbf{\Omega}_{LR})$, in Eq. (12) transforms the L frame to the R frame via a set of Euler angles, $\mathbf{\Omega}_{LR}$.

The diffusion operator for a cylindrical molecule undergoing a Brownian rotation in an isotropic medium is given by

$$\hat{\Gamma}(\Omega) = \hat{J}\cdot R\cdot\hat{J}. \tag{13}$$

Here the operator $\hat{J}$, defined in the R frame, is the generator of an infinitesimal rotation of the molecule. The diffusion operator R is diagonal in the R frame and has two principal components, $R_\perp$ and $R_\parallel$ describing, respectively, the tumbling and spinning motion of the molecule. The more general form of Eq. (13) appropriate for an anisotropic fluid is given elsewhere [27].

To proceed, we need to define a basis set in Liouville space to calculate the matrix elements of $\hat{\mathscr{L}}(\Omega)$ and its eigenfunctions and eigenvalues in Eq. (11). It may be written as a direct product of a spin portion and an angular portion

$$|p^S, q^S, p^I, q^I; L, M, K\rangle = |p^S, q^S, p^I, q^I\rangle \times \frac{[L(L+1)]^{1/2}}{8\pi^2}\mathscr{D}^{L}_{MK}(\mathbf{\Omega}_{LR}). \tag{14}$$

Here the electron spin-transition numbers $p^S = m'_S - m''_S$ and $q^S = m'_S + m''_S$, where m'_S and m''_S are electron spin-quantum numbers before and after the transition, respectively. Equivalent definitions hold for the nuclear spin. For a system of one electron spin ($S = 1/2$), such as a nitroxide, we may have $p^S = \pm 1$ denoting the two counter rotating xy components of the electron spin magnetization, and $p^S = 0$ representing its z component. The matrix elements of $\hat{\mathscr{H}}^{\mathrm{x}}$ and $\hat{\Gamma}$ in the basis set given by Eq. (14) can be found in [27].

The basis set defined in Eq. (14) is particularly convenient in the high field limit and in the absence of the microwave field. It can then easily be shown that, expressed in this basis set, the stochastic Liouville operator is block diagonal with respect to different p^S values,

$$O\mathrm{e}^{-\Lambda t}O^{\mathrm{tr}} = \begin{pmatrix} O_{-1}\mathrm{e}^{-\Lambda_{-1}t}O^{\mathrm{tr}}_{-1} & 0 & 0 \\ 0 & O_0\mathrm{e}^{-\Lambda_0 t}O^{\mathrm{tr}}_0 & 0 \\ 0 & 0 & O_{+1}\mathrm{e}^{-\Lambda_{+1}t}O^{\mathrm{tr}}_{+1} \end{pmatrix}. \tag{15}$$

Eq. (11) may then be decomposed into three equations

$$\hat{\chi}_m(\Omega, t+t_0) = O_m\mathrm{e}^{-\Lambda_m t}O^{\mathrm{tr}}_m\hat{\chi}_m(\Omega, t_0), \tag{16}$$

where $m \equiv p_S = \pm 1, 0$, and the matrix of eigenfunctions O_m and the diagonal matrix of eigenvalues Λ_m may be computed separately in their respective basis sets.

2.3. Pulse propagator superoperator

Let us next consider the three $\pi/2$ pulses in Fig. 1. In this section, they are treated as ideal pulses which are very strong and of very short duration. During the pulses the interaction between the electron spin and the microwave radiation is thus so dominant that the effects of $\hat{\mathscr{H}}_0$ (in the rotating frame, see below) and of $\hat{\Gamma}$can be completely ignored. Thus $\hat{\mathscr{H}}^{\mathrm{x}}_1$ is the only term in Eq. (1) which is significant, so we write for the rotating frame

$$\frac{\partial}{\partial t}\hat{\rho}(t) = -\mathrm{i}\hat{\mathscr{H}}^{\mathrm{x}}_{1,\mathrm{rot}}\hat{\rho}(t). \tag{17}$$

The formal solution to Eq. (17) for a pulse of duration t_p can be written as

$$\hat{\rho}(t_0+t_p) = \exp[-\mathrm{i}\hat{\mathscr{H}}^{\mathrm{x}}_{1,\mathrm{rot}}t_p]\hat{\rho}(t_0) \equiv \hat{\mathscr{P}}(t_p)\hat{\rho}(t_0), \tag{18}$$

where the pulse propagator superoperator, $\hat{\mathscr{P}}(t_p)$, has been defined. Since Eq. (17) has been written in the appropriate rotating frame, $\hat{\mathscr{H}}^{\mathrm{x}}_{1,\mathrm{rot}}$ is time independent. It should also be noted from a comparison of Eqs. (10) and (18), that while it is more convenient to work with the reduced density matrix $\hat{\chi}$ in the absence of a microwave pulse, the time evolution during a strong pulse is best described in terms of the conventional density matrix $\hat{\rho}$.

Now we may write the pulse Hamiltonian in the rotating frame [13]

$$\hat{\mathscr{H}}_{1,\mathrm{rot}} = \frac{\omega_1}{2}(S_+ e^{-i\phi} + S_- e^{i\phi}), \tag{19}$$

where ω_1 is the angular frequency and ϕ the phase of the microwave radiation. For a strong pulse of duration t_p, we have

$$\theta = \omega_1 t_p = \gamma_e B_1 t_p, \tag{20}$$

where θ is the flip angle of the pulse, γ_e the gyromagnetic ratio of the electron spin and B_1 the intensity of the pulse. From Eqs. (14) and (18)–(20), the matrix elements of the pulse propagator superoperator can be shown to have the following structure when expressed in the electron spin portion, $|p^S, q^S\rangle$, of the basis set in Eq. (14):

$$\hat{\mathscr{P}}(\theta,\phi) = \begin{array}{c} \begin{array}{cccc} |0,1\rangle & |0,-1\rangle & |1,0\rangle & |-1,0\rangle \end{array} \\ \begin{pmatrix} \cos^2(\theta/2) & \sin^2(\theta/2) & \frac{i}{2}\sin\theta e^{i\phi} & -\frac{i}{2}\sin\theta e^{-i\phi} \\ \sin^2(\theta/2) & \cos^2(\theta/2) & -\frac{i}{2}\sin\theta e^{i\phi} & \frac{i}{2}\sin\theta e^{-i\phi} \\ \frac{i}{2}\sin\theta e^{-i\phi} & -\frac{i}{2}\sin\theta e^{-i\phi} & \cos^2(\theta/2) & \sin^2(\theta/2)e^{-i2\phi} \\ -\frac{i}{2}\sin\theta e^{i\phi} & \frac{i}{2}\sin\theta e^{i\phi} & \sin^2(\theta/2)e^{i2\phi} & \cos^2(\theta/2) \end{pmatrix} \end{array}, \tag{21}$$

and it is block diagonal in the nuclear spin and molecular reorientation spaces. The effects of a microwave pulse can then be fully specified by Eq. (21). For example, $\langle p_1^S, q_1^S|\hat{\mathscr{P}}|p_2^S, q_1^S\rangle = \hat{\mathscr{P}}_{(p_2^S \leftarrow p_1^S)}$, represents the pulse whose propagator transforms the density matrix from the p_1^S space into the p_2^S space.

Starting from ρ_{eq} and applying to it Eqs. 21 and 16 repeatedly, the time evolution of the density matrix for the coherence pathways defined in Fig. 1 can be expressed as

$$\begin{aligned} \rho_{\mp}(t_1 + T + t_2) = {} & O_{-1}\exp[-\Lambda_{-1}t_2]O_{-1}^{\mathrm{tr}}\hat{\mathscr{P}}_{(-1\leftarrow 0)}O_0 \\ & \times \exp[-\Lambda_0 T]O_0^{\mathrm{tr}} \times \hat{\mathscr{P}}_{(0\leftarrow \mp 1)}O_{\mp 1} \\ & \times \exp[-\Lambda_{\mp 1}t_1]O_{\mp 1}^{\mathrm{tr}}\hat{\mathscr{P}}_{(\mp 1\leftarrow 0)}\rho_{\mathrm{eq}}. \end{aligned} \tag{22}$$

The ESR signal can then be computed from

$$S_{c\pm}^{\text{2D-ELDOR}} = Tr[S_-\rho_{\mp}] \tag{23}$$

2.4. Arbitrary pulses of finite intensity

2.4.1. Trotter formula

For a pulse of finite intensity, the effect of $\hat{\mathscr{H}}_0$ (in the rotating frame) as well as molecular rotational dynamics cannot be ignored during the pulse. In this case, $\hat{\mathscr{H}}_1$ becomes comparable with (or even smaller than) $\hat{\mathscr{H}}_0$ and/or $\hat{\Gamma}$ in Eq. (1), and we must solve the complete equation of motion without dropping off any terms. We now rewrite Eq. (1) as (in the rotating frame)

$$\frac{\partial}{\partial t}\hat{\rho}(\Omega,t) = [-\hat{\mathscr{L}}(\Omega) - i\hat{\mathscr{H}}^{\times}_{1,\mathrm{rot}}][\hat{\rho}(\Omega,t) - \hat{\rho}_{\mathrm{eq}}(\Omega,t)]. \tag{24}$$

While an exact formal solution to Eq. (24) may be written, the computation of the relevant eigenfunctions and eigenvalues could be formidable. The three coherence modes ($m = 0, \pm 1$, cf. Fig. 1) in Eq. (16) couple to each other due to the presence of the pulse propagator and one has to solve the full eigen-equation of much larger dimension.

A useful technique for dealing with Eq. (24) is the so-called split operator method [18], which is based on the Trotter formula [19,20]

$$\exp[A+B] = \lim_{n\to\infty}\left(\exp\left[\frac{A}{n}\right]\exp\left[\frac{B}{n}\right]\right)^n \tag{25}$$

for operators A and B. Eq. (24) can be used advantageously to separate the effects of non-commuting operators. When applied to the propagator relevant to the case of pulses, of finite intensity, the Trotter formula takes on the following form:

$$\begin{aligned} \exp[(-\hat{\mathscr{L}} - i\hat{\mathscr{H}}^{\times}_1)t_p] &= \lim_{n\to\infty}(\exp[-\hat{\mathscr{L}}\Delta t]\exp[-i\ \hat{\mathscr{H}}^{\times}_1\Delta t])^n \\ &= \lim_{n\to\infty}(\exp[-i\ \hat{\mathscr{H}}^{\times}_1\Delta t]\exp[-\hat{\mathscr{L}}\Delta t])^n, \end{aligned} \tag{26}$$

where $\Delta t = t_p/n$, and we have dropped the subscript *rot* for convenience. (The first case follows if $A \to \hat{\mathscr{L}}$ and the second if $B \to \hat{\mathscr{L}}$.) In Eq. (26), the original arbitrary pulse of duration t_p has been approximated by a sequence of short pulses of duration Δt interspersed by free evolution periods also of duration Δt. Thus, by breaking the original pulse width t_p into n very small time intervals, the stochastic Liouville operator and the pulse propagator can be treated as though they commute. Within each time interval, the effects of pulse and of free precession with spin relaxation/molecular rotational dynamics on the time evolution of the spin density operator may be treated independently as distinct exponential operators, which are each then applied n times, by using Eqs. (17) and (10), respectively.

2.4.2. Equation of motion

In this section, we will solve the equation of motion for an arbitrary pulse whose width is t_p and whose intensity is B_1. To apply the Trotter formula, the pulse is divided into n steps of spacing Δt. We start just before the pulse, where the spin density operator is $\hat{\rho}(\Omega, t_0)$. During the initial Δt, the electron spin magnetization is first allowed to undergo the combined process of spin evolution and molecular rotation while ignoring the pulse, (i.e., the second form of Eq. (26)). Thus, the reduced spin density operator after this period is given by Eq. (10)

$$\hat{\chi}(\Omega, t_1) = \exp[-\hat{\mathscr{L}}(\Omega)\Delta t][\hat{\rho}(\Omega, t_0) - \hat{\rho}_{\mathrm{eq}}(\Omega)], \tag{27}$$

where $t_1 = t_0 + \Delta t$. One then follows with a pulse of duration over the same Δt, which rotates the electron spin magnetization by an angle $\Delta\theta$ (see Eq. (20)):

$$\Delta\theta = \gamma_e B_1 \Delta t. \tag{28}$$

The spin density operator after the pulse can be written according to Eq. (18)

$$\hat{\rho}(\Omega, t_1) = \hat{\mathscr{P}}(\Delta t)[\hat{\chi}(\Omega, t_1) + \hat{\rho}_{\mathrm{eq}}(\Omega)] \tag{29}$$

with $\hat{\chi}(\Omega, t_1)$ given by Eq. (27), so that Eq. (29) becomes

$$\begin{aligned}\hat{\rho}(\Omega, t_1) &= \hat{\mathscr{P}}(\Delta t)\exp[-\hat{\mathscr{L}}(\Omega)\Delta t]\hat{\rho}(\Omega, t_0) + \hat{\mathscr{P}}(\Delta t) \\ &\quad \times (1 - \exp[-\hat{\mathscr{L}}(\Omega)\Delta t])\hat{\rho}_{\mathrm{eq}}(\Omega) \\ &\equiv \hat{M}(\Omega, \Delta t)\hat{\rho}(\Omega, t_0) + \hat{N}(\Omega, \Delta t)\hat{\rho}_{\mathrm{eq}}(\Omega),\end{aligned} \tag{30}$$

In Eq. (30), two new operators

$$\hat{M}(\Omega, \Delta t) \equiv \hat{\mathscr{P}}(\Delta t)\exp[-\hat{\mathscr{L}}(\Omega)\Delta t] \tag{31}$$

and

$$\hat{N}(\Omega, \Delta t) \equiv \hat{\mathscr{P}}(\Delta t)(1 - \exp[-\hat{\mathscr{L}}(\Omega)\Delta t]) \tag{32}$$

have been introduced. $\hat{M}(\Omega, \Delta t)$ represents the propagator driving the spin density operator from $\hat{\rho}(\Omega, t_0)$ to $\hat{\rho}(\Omega, t_1)$ during Δt; $\hat{N}(\Omega, \Delta t)$ is due to the switching back and forth between $\hat{\rho}$ and $\hat{\chi}$, as required when applying $\hat{\mathscr{P}}(\Delta t)$ and $\exp[-\hat{\mathscr{L}}(\Omega)\Delta t]$ separately (see Eqs. (10) and (18)). It arises because the stochastic Liouville operator seeks to return $\hat{\rho}$ to its thermal equilibrium value, ρ_{eq} (cf. Eq. (10)), whereas the radiation term, yielding the pulse propagator, seeks to remove the system from thermal equilibrium (cf. Eq. (18)). (Eq. (30) can be shown to be equivalent, for very small Δt, to the integrated form of Eq. (24) by expanding the exponential operators and keeping only terms no higher than linear in Δt).

During the second Δt, the relation equivalent to Eq. (30) can be written between $\hat{\rho}(\Omega, t_2)$ and $\hat{\rho}(\Omega, t_1)$, and upon replacing $\hat{\rho}(\Omega, t_1)$ with Eq. (30), we have

$$\begin{aligned}\hat{\rho}(\Omega, t_2) &= \hat{M}^2(\Omega, \Delta t)\hat{\rho}(\Omega, t_0) \\ &\quad + [\hat{M}(\Omega, \Delta t) + 1]\hat{N}(\Omega, \Delta t)\hat{\rho}_{\mathrm{eq}}(\Omega).\end{aligned} \tag{33}$$

The same procedure is repeated n times until the final $\hat{\rho}(\Omega, t_n)$ is reached

$$\begin{aligned}\hat{\rho}(\Omega, t_p) &= \hat{\rho}(\Omega, t_n) \\ &= \hat{M}^n(\Omega, \Delta t)\hat{\rho}(\Omega, t_0) \\ &\quad + \left[\sum_{i=1}^{n} \hat{M}^{i-1}(\Omega, \Delta t)\right]\hat{N}(\Omega, \Delta t)\hat{\rho}_{\mathrm{eq}}(\Omega),\end{aligned} \tag{34}$$

where $\hat{M}^n(\Omega, \Delta t)$ and $\hat{M}^{i-1}(\Omega, \Delta t)$ refer to $\hat{M}(\Omega, \Delta t)$ being applied n times and $i - 1$ times, respectively.

In arriving at Eq. (34), $\exp[-\hat{\mathscr{L}}\Delta t]$ was applied before $\hat{\mathscr{P}}(\Delta t)$ on the initial density operator $\hat{\rho}(\Omega, t_0)$ (i.e., the second form of Eq. (26)). On the other hand, if we start with $\hat{\mathscr{P}}(\Delta t)$ (i.e., the first form of Eq. (26)), a result similar to Eq. (34) is obtained, except that $\hat{N}(\Omega, \Delta t)$ is now defined as

$$\hat{N}'(\Omega, \Delta t) = 1 - \exp[-\hat{\mathscr{L}}(\Omega)\Delta t] \tag{35}$$

instead of $\hat{\mathscr{P}}(\Delta t)(1 - \exp[-\hat{\mathscr{L}}(\Omega)\Delta t])$ in Eq. (32). From the definition of $\hat{\mathscr{P}}(\Delta t)$, and expanding the exponential operators in a Taylor's series and neglecting the second and higher order terms for the very small time interval Δt, it can easily be shown that the two definitions of $\hat{N}(\Omega, \Delta t)$ given by Eqs. (32) and (35) become the same. This clearly illustrates that $\exp[-\hat{\mathscr{L}}\Delta t]$ and $\hat{\mathscr{P}}(\Delta t)$ commute with each other if Δt is sufficiently small. (This is mathematically equivalent to the well known fact that unitary operators representing rotations do not commute in general, but they do commute for infinitesimal rotations).

2.4.3. 2D-ELDOR ESR signals

Having determined the density operator for arbitrary (or imperfect) pulses, we now proceed to compute the 2D-ELDOR ESR signals. For the pulse sequence given in Fig. 1, the final density operator may be obtained by applying Eqs. (11) and (34)

$$\begin{aligned}\rho_{\mp}(t_1 + T + t_2 + 3t_p) = P_0^{1/2}(\Omega) \\ \times O_{-1}\exp[-\Lambda_{-1}t_2]O_{-1}^{\mathrm{tr}}\hat{\rho}_{(-1\leftarrow 0)}(\Omega, t_p) \\ \times O_0\exp[-\Lambda_0 T]O_0^{\mathrm{tr}}\hat{\rho}_{(0\leftarrow\mp 1)}(\Omega, t_p) \\ \times O_{\mp 1}\exp[-\Lambda_{\mp 1}t_1]O_{\mp 1}^{\mathrm{tr}}\hat{\rho}_{(\mp 1\leftarrow 0)}(\Omega, t_p)P_0^{-1/2}(\Omega)\rho_{\mathrm{eq}},\end{aligned} \tag{36}$$

where the equilibrium molecular angular distribution, $P_0(\Omega)$, has been defined in Eq. (6) and is inserted here to symmetrize the diffusion operator (which is needed for anisotropic fluids (cf. [21,23,27])).

$$\hat{\tilde{\Gamma}}(\Omega) = P_0^{-1/2}(\Omega)\hat{\Gamma}(\Omega)P_0^{1/2}(\Omega). \tag{37}$$

The $\hat{\rho}_{(j\leftarrow i)}(\Omega, t_p)$'s in Eq. (36) are submatrices of $\hat{\rho}(\Omega, t_p)$ in Eq. (34), which contains all the information about the imperfect pulse. For example, the second pulse in Fig. 1 is described by $\hat{\rho}_{(0\leftarrow\mp 1)}(\Omega, t_p)$. To construct the $\hat{\rho}(\Omega, t_p)$ matrix, we need to calculate the matrix elements of $\hat{M}(\Omega, \Delta t)$ and $\hat{N}(\Omega, \Delta t)$ defined in Eqs. 31 and 35, respectively. In terms of the eigenmodes of the stochastic Liouville superoperator given in Eq. (11), the operators $\hat{M}(\Omega, \Delta t)$ and $\hat{N}(\Omega, \Delta t)$ may be expressed in the basis set in Eq. (14) as:

$$\begin{aligned}\hat{M}(\Omega, \Delta t) &= \exp[-\hat{\mathscr{L}}(\Omega)\Delta t]\hat{\mathscr{P}}(\Delta t) \\ &\begin{pmatrix} O_{-1}e^{-\Lambda_{-1}\Delta t}O_{-1}^{\mathrm{tr}}P_{-1-1} & O_{-1}e^{-\Lambda_{-1}\Delta t}O_{-1}^{\mathrm{tr}}P_{-10} & O_{-1}e^{-\Lambda_{-1}\Delta t}O_{-1}^{\mathrm{tr}}P_{-11} \\ O_0e^{-\Lambda_0\Delta t}O_0^{\mathrm{tr}}P_{0-1} & O_0e^{-\Lambda_0\Delta t}O_0^{\mathrm{tr}}P_{00} & O_0e^{-\Lambda_0\Delta t}O_0^{\mathrm{tr}}P_{01} \\ O_1e^{-\Lambda_1\Delta t}O_1^{\mathrm{tr}}P_{1-1} & O_1e^{-\Lambda_1\Delta t}O_1^{\mathrm{tr}}P_{10} & O_1e^{-\Lambda_1\Delta t}O_1^{\mathrm{tr}}P_{11} \end{pmatrix},\end{aligned} \tag{38}$$

where the P_{ij}s are the submatrices of the pulse propagator matrix given in Eq. (21) and can be obtained from Eq. (21) with θ being replaced by $\Delta\theta$, which is related to Δt via Eq. (28):

$$P_{00} = \begin{pmatrix} \cos^2(\Delta\theta/2) & \sin^2(\Delta\theta/2) \\ \sin^2(\Delta\theta/2) & \cos^2(\Delta\theta/2) \end{pmatrix}, \quad P_{\pm1\pm1} = \cos^2(\Delta\theta/2), \quad P_{\pm1\mp1} = \sin^2(\Delta\theta/2)e^{\mp i2\phi},$$
$$P_{0\pm1} = \begin{pmatrix} \pm\frac{i}{2}\sin\Delta\theta e^{\mp i\phi} \\ \mp\frac{i}{2}\sin\Delta\theta e^{\mp i\phi} \end{pmatrix}, \quad P_{\pm10} = \begin{pmatrix} \pm\frac{i}{2}\sin\Delta\theta e^{\pm i\phi} \\ \mp\frac{i}{2}\sin\Delta\theta e^{\pm i\phi} \end{pmatrix}^{tr}. \tag{39}$$

Note that the diagonal and off-diagonal spaces couple to each other due to the presence of the pulse propagator, as is seen from Eq. (38). Thus, to follow the time evolution of the spin density operator within a finite pulse, one has to perform a number of matrix-matrix multiplications in the full space, which involve all the elements of pulse propagator in Eq. (21). This is in contrast to the case of an ideal (or very strong) pulse, where only a single pulse matrix element is needed. It can easily be shown that the matrix-matrix multiplications in $\hat{M}^n$ (cf. Eq. (34)) do not alter the phase of the pulses. The corresponding matrix elements of operator $\hat{N}(\Omega,\Delta t)$ have the following form (to lowest order in Δt, cf. above):

$$\hat{N}(\Omega,\Delta t) = \hat{N}'(\Omega,\Delta t) = 1 - \exp[-\hat{\mathscr{L}}(\Omega)\Delta t] = \begin{pmatrix} 1 - O_{-1}e^{-\Lambda_{-1}\Delta t}O_{-1}^{tr} & 0 & 0 \\ 0 & 1 - O_0 e^{-\Lambda_0\Delta t}O_0^{tr} & 0 \\ 0 & 0 & 1 - O_1 e^{-\Lambda_1\Delta t}O_1^{tr} \end{pmatrix}. \tag{40}$$

Finally, the 2D-ELDOR ESR signal can be calculated from Eq. (23).

3. Results and discussion

3.1. Simulation methods

Simulations of CW spectra are normally performed in the off-diagonal electron spin space $|\pm1,0\rangle$ (cf. Eq. (14)) and no knowledge about the diagonal subspace $|0,\pm1\rangle$ is required. However, in the 2D-ELDOR experiment in Fig. 1, the microwave pulse switches the electron magnetization between the off-diagonal and diagonal spaces and the full electron spin space covering both subspaces has to be considered as given in Eq. (36). During the three time intervals when the microwave field is absent, the matrix of stochastic Liouville superoperator is block diagonal in the electron spin space, as can be seen in Eq. (15), which greatly simplifies the calculation of the relevant eigenvectors and eigenvalues. During the pulses, if they are assumed to be perfect, that is, if they are sufficiently strong in intensity and short in duration, the time evolution of the electron spin can be followed by Eq. (18).

In the present work, we are dealing with arbitrary pulses of finite intensity B_1 and pulse width t_p, during which both electron spin relaxation and molecular reorientation may take place. This complex problem has been simplified by applying the Trotter formula, which requires dividing the pulse width into small time intervals. In each time interval, the Trotter formula allows a decoupling of stochastic Liouville operator from the pulse propagator (Eq. (25)). It follows that the stochastic Liouville operator and pulse propagator can be treated independently using Eqs. 10 and 18, respectively.

The 2D-ELDOR spectral simulation starts with the stochastic Liouville operator $\hat{\mathscr{L}}$ in Eq. (8), with the spin Hamiltonian $\hat{\mathscr{H}}$ given in Eq. (12) and the diffusion operator $\hat{\Gamma}$ given in Eq. (13). The matrix elements of the stochastic Liouville operator are first computed in the off-diagonal subspace $|\pm1,0,p^I,q^I;L,M,K\rangle$ and the diagonal subspace $|0,\pm1,p^I,q^I;L,M,K\rangle$ of the basis set defined in Eq. (14). In general, the matrix dimension of $\hat{\mathscr{L}}$ in the diagonal space, n_d, is approximately two times larger than that of the off-diagonal space, n_o. Since the stochastic Liouville matrix is block diagonal with respect to the two subspaces, the three stochastic Liouville sub matrices can be diagonalized independently to yield the eigenfunctions and eigenvalues, O_0 and λ_0 for the diagonal space, and $O_{\pm1}$ and $\lambda_{\pm1}$ for the off-diagonal space, respectively. In this work, the Rutishauser algorithm was used for the diagonalization of the stochastic Liouville matrices, since it produces exact eigenfunctions and eigenvalues [14] and is a better choice than the Lanczos algorithm when the molecular reorientational rate is slow.

Having calculated the eigenfunction and eigenvalue matrices, we are now able to construct the matrices for the $\hat{M}$ and $\hat{N}$ operators, using Eqs. 38 and 40, respectively. Note that unlike the stochastic Liouville matrix, the $\hat{M}$ matrix is not block diagonal with respect to the electron spin space, due to the presence of the pulse. Thus we are dealing with a matrix which is four times (or two times) larger than the off-diagonal (or diagonal) of the stochastic Liouville matrices, respectively. We can immediately see the computational challenge when calculating the spin density operator $\hat{\rho}(\Omega,t_p)$ in Eq. (34). One way to avoid directly computing $\hat{M}^n$ is by computing the matrix-vector multiplications such as $\hat{M}(\Omega,\Delta t)\hat{\rho}(\Omega,t_0)$. However, this sequence of matrix-vector multiplications would have to be repeated for each of the three arbitrary microwave pulses in Fig. 1, since they start from different t_0. On the other hand, if we compute $\hat{M}^n$ directly, it only needs to be performed once and only one portion of the $\hat{M}^n$ matrix is needed for each pulse. In addition, we actually only need to compute $m = \log(n)/\log(2)$, instead of $m = (n-1)$, matrix–matrix multiplies to obtain $\hat{M}^n$, by a process of successive squaring. For example, if $n = 8$, m is only 3.

It should be noted that the Trotter formula in its symmetrized form

$$\exp[A+B] = \lim_{n\to\infty}\left(\exp\left[\frac{B}{2n}\right]\exp\left[\frac{A}{n}\right]\exp\left[\frac{B}{2n}\right]\right)^n \tag{41}$$

converges faster than does Eq. (25). Eq. (41) has been used in most previous works [18,13]. In an analytic study, Salikhov et al. [18] used n values of 2–4, while in another study by Saxena and Freed [13], it was found that a value of 8 for n was sufficient for the numerical convergence (at 9 GHz) when $B_1 = 17.8$ G and for a pulse ten times weaker ($B_1 = 1.78$ G), $n = 16$ should be used. (These previous studies did not include the stochastic operator $\hat{\Gamma}$, so they did not require the SLE). In the present study, we used the original form of the Trotter formula given in Eq. (25). Although the symmetrized form converges faster, it requires more matrix–matrix multiplications, which is the major consideration when the stochastic Liouville matrix becomes extremely large. For a radiation field of $B_1 = 17.8$ G, $n = 8$ is sufficient in a typical slow motional 2D-ELDOR spectral simulation (for 9 GHz).

3.2. Theoretical simulations

We apply the theory developed in this work, by studying the effects of pulse width on the 2D-ELDOR ESR spectra. In the spectral simulations in this section, we use the following magnetic parameters: $A_{xx} = 5.5$ G, $A_{yy} = 5.7$ G, $A_{zz} = 35.8$ G, $g_{xx} = 2.0084$, $g_{yy} = 2.0060$, and $g_{zz} = 2.0022$, which are typical for a nitroxide spin label (cf. next section). The static magnetic field is $B_0 = 3280$ G, corresponding to 9.2 GHz (except where noted). The other parameters related to a 2D-ELDOR spectral simulation are: dead times $t_{01} = 50$ ns and $t_{02} = 50$ ns (except where noted) and mixing time $T_m = 100$ ns, which are typical experimental values (cf. next section).

We present, in Figs. 2–4, simulated 9.2 GHz ESR spectra characteristic of the range of rotational rates encountered in studies of nitroxide spin labels. Fig. 2 shows the simulated 2D-ELDOR spectra for different pulse widths in the motional narrowing regime. Here an isotropic rotational diffusion constant of $R_0 = 1 \times 10^{11}$ s^{-1} is used. This motion is fast enough to average out the anisotropy of the A and g tensors and only the isotropic hyperfine coupling, a_0, determines the line positions. In a CW 9-GHz experiment, this usually results in a spectrum with three well separated peaks of almost equal intensity. The same is observed for the auto-peaks in the 9 GHz 2D-ELDOR spectrum in

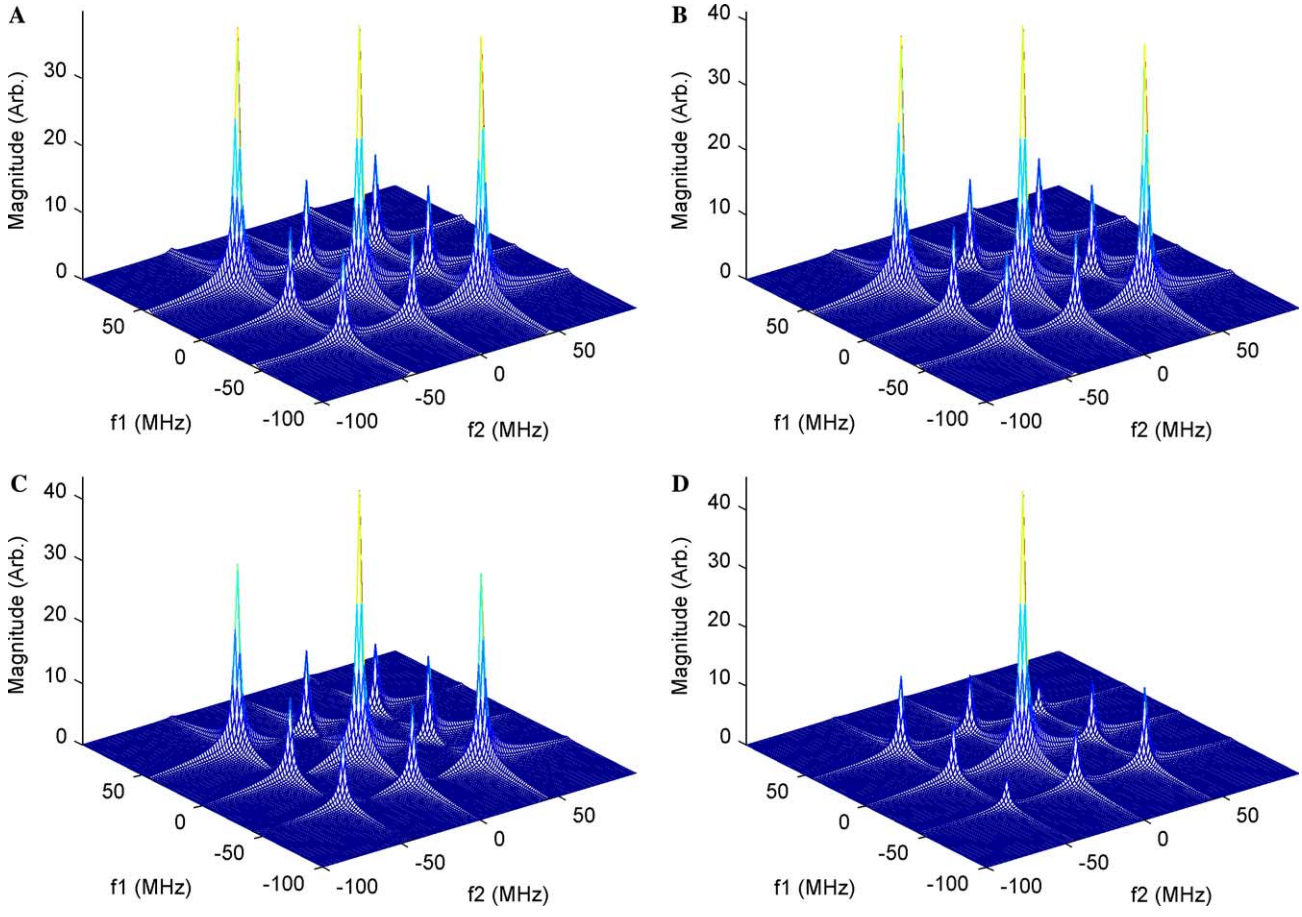

Fig. 2. Theoretical 9 GHz 2D-ELDOR spectra showing the effect of the pulse width in the motional narrowing region: $R_0 = 1 \times 10^{11}$ s^{-1}, $\omega_{HE} = 1 \times 10^7$ s^{-1}, $\Delta_G = 0.1$ G. $t_p =$ (A) 0 ns, i.e., ideal pulse, (B) 5 ns, (C) 10 ns, and (D) 15 ns.

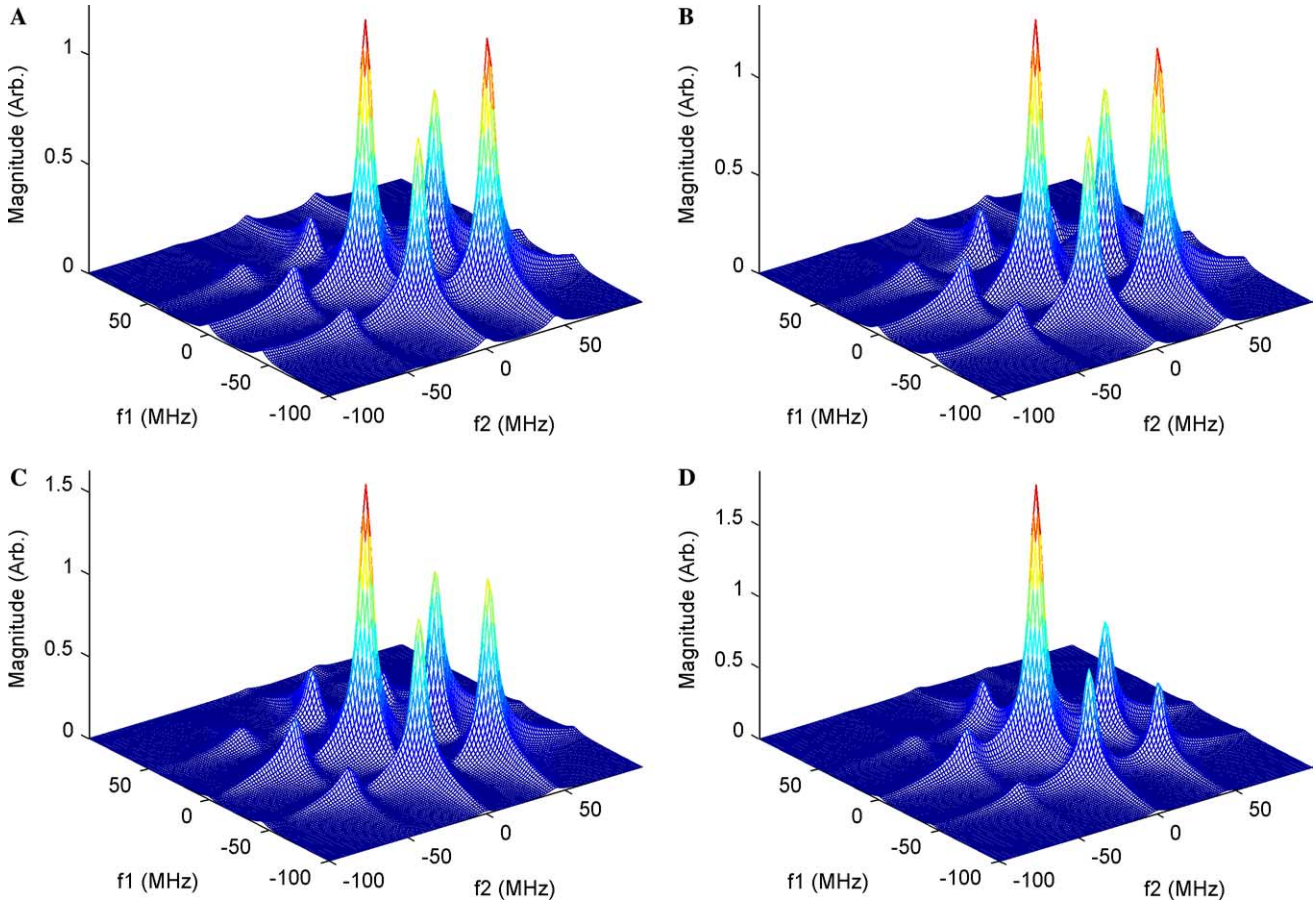

Fig. 3. Theoretical 9 GHz 2D-ELDOR spectra showing the effect of the pulse width in the incipient slow motional region: $R_0 = 3.2 \times 10^8\ s^{-1}$, $\omega_{HE} = 1 \times 10^7\ s^{-1}$, $\Delta_G = 0.3$ G. $t_p =$ (A) 0 ns, (B) 5 ns, (C) 10 ns, and (D) 15 ns.

Fig. 2A, that was calculated for ideal pulses, where the separation between the two outer peaks is $2a_0 = 31.3$ G. In addition, there are $\Delta m_{\pm} = \pm 1$ and ± 2 cross peaks arising mainly from the HE, ($\omega_{HE} = 1 \times 10^7\ s^{-1}$), which is a typical value in, e.g., a lipid membrane [7]. We checked that 1 ns $\pi/2$ pulses, corresponding to a B_1 of about 89 G, which is more than sufficient to cover the bandwidth of 15.6 G in Fig. 2A, are for all practical purposes ideal pulses, by comparison with the standard 2D-ELDOR computational routines [14,15]. When the $\pi/2$ pulse widths are increased to 5 ns (corresponding to $B_1 \approx 18$ G), the simulated spectrum in Fig. 2B does not show much difference from that in Fig. 2A. This indicates that a pulse duration of 5 ns is close to an ideal pulse in the motional narrowing regime at 9 GHz for nitroxides.

When the pulse widths are further increased to 10 ns, the simulated spectrum in Fig. 2C differs significantly from those in Figs. 2A and 2B. It can be seen from Fig. 2C that there is an intensity loss in both outer auto-peaks. The applied field B_1 of 8.9 G generating a 10 ns $\pi/2$ pulse is insufficient to fully excite the ± 15.6 G bandwidth. A further reduction in intensity of the outer auto and the cross peaks is observed in Fig. 2D, where the pulse width is 15 ns corresponding to a B_1 of about 6 G. Naturally, the central auto-peak, which is at $f_1 = f_2 \approx 0$ MHz, is unaffected by the increased duration of the $\pi/2$ pulses.

The same simulations were repeated for a slower motional rate constant of $3.2 \times 10^8\ s^{-1}$, and the results are shown in Fig. 3. Now the molecular reorientation is not fast enough to fully average out the magnetic anisotropy, and much broader peaks are observed. Also, the cross-peaks are now largely determined by nuclear spin flips induced by rotational modulation of the hyperfine tensor. In the case of an ideal pulse in Fig. 3A, the three peaks have different intensities due to the incomplete averaging. A small but noticeable reduction in the outer peak intensities is seen in Fig. 3B as the pulse widths increase to 5 ns. This is an indication that the 5 ns pulses may not be nearly as ideal in the incipient slower motional regime as in the motional narrowing regime, possibly due to finite effects of relaxation during the pulse. As t_p becomes longer and the B_1 is weaker, further intensity reduction in the outer peaks is observed in Figs. 3C and D. In the latter case, the overall pattern of peaks becomes substantially different from that of Fig. 3A.

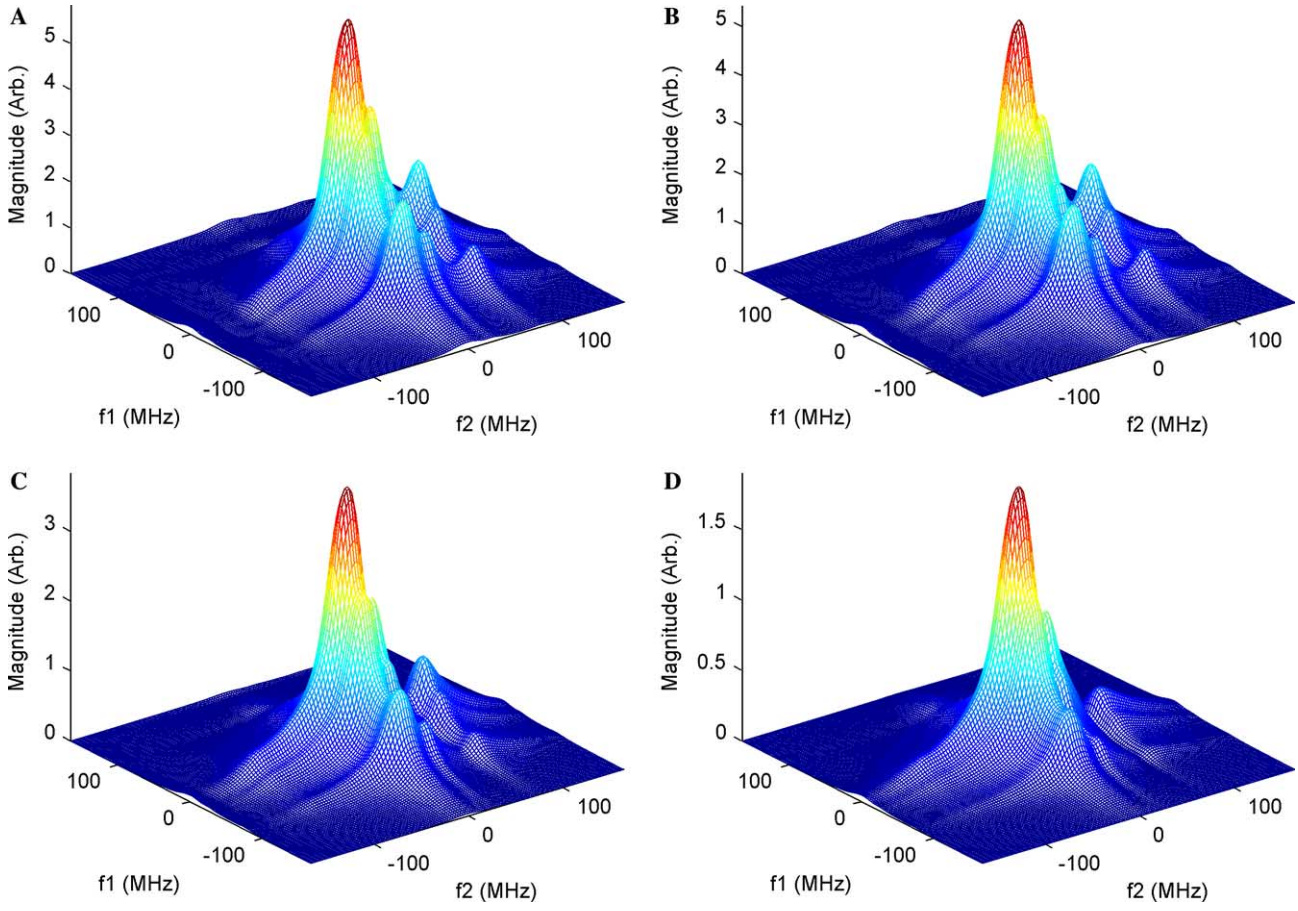

Fig. 4. Theoretical 9 GHz 2D-ELDOR spectra showing the effect of the pulse width in the slow motional region: $R_0 = 1 \times 10^7\ s^{-1}$, $\omega_{HE} = 1 \times 10^6\ s^{-1}$, $\Delta_G = 0.3$ G. $t_p =$ (A) 0 ns, (B) 5 ns, (C) 15 ns, and (D) 30 ns. The dead times: $t_{01} = t_{02} = 25$ ns.

In Fig. 4 we show results for an $R_o = 1 \times 10^7\ s^{-1}$, which is well into the slow-motional regime. The 2D-ELDOR auto- and cross-peaks are very broad, as expected for this case, which is near the T_2 minimum (ca. 15 ns, cf. [16]). Here, we find that the 2D-ELDOR spectra are less sensitive to increasing the pulse width. Only modest differences are noted for a 15 ns pulse width vs. a strong pulse. Substantial effects are, however, seen for long pulse widths of 30 ns. The reduced sensitivity to pulse width may be explained by the fact that the dynamic spin packets making up the 2D-ELDOR spectrum have very short T_2's resulting in very large homogeneous broadening. Their breadth means that the peaks that are not centered near the middle of the spectrum are, in effect, not substantially displaced in frequency from the applied microwave frequency, i.e., their (homogeneous) wings extend into the central region of the spectrum. Thus spectral coverage in this motional regime does not appear to be a concern.

It is of interest to study the effects of pulse width for higher frequency 2D-ELDOR ESR which is sensitive to faster motions. Fig. 5 displays the variation of 95 GHz 2D-ELDOR spectra with pulse width for $R_0 = 3.2 \times 10^9\ s^{-1}$. In contrast to the 9 GHz cases, with ideal $\pi/2$ pulses, the higher frequency auto-peak is the most intense instead of the central auto-peak (cf. Fig. 5A). This is due to the greatly increased role of the g-tensor in the spin relaxation. It also leads to increased broadening of all auto and cross peaks. As the pulse width is increased (cf. Figs. 5B–D), the intensity of the central peak is unaffected as before, but the intensity of the outer peaks is reduced, so that for a 15 ns pulse width the central peak is a little more intense than the high-frequency auto-peak. The spectral pattern of Fig. 5D becomes substantially different from that arising from ideal $\pi/2$ pulses. However, as for the 9 GHz cases, there is only a small difference between Fig. 5B corresponding to 5 ns pulse widths and Fig. 5A for ideal pulses.

We now note what effects on the estimation of the molecular motion would result if one treats an arbitrary pulse as an ideal one. From the above analysis, both incipient slow motion and a non-ideal pulse have the similar effect of causing intensity reductions in the outer peaks. If a simulation program assuming ideal pulses is used, the molecular motional rate may be

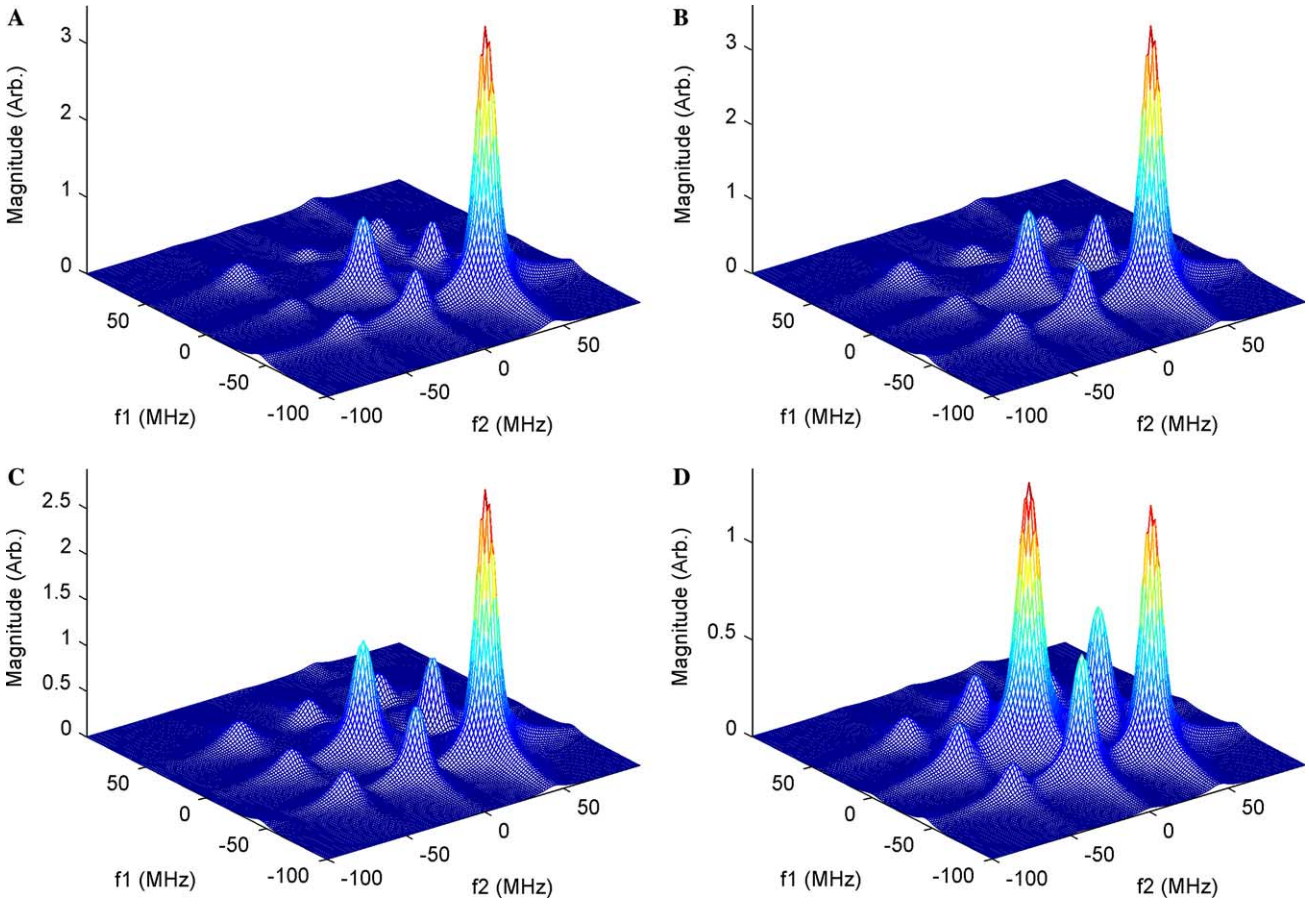

Fig. 5. Theoretical 95 GHz 2D-ELDOR spectra showing the effect of the pulse width in the incipient slow motional region: $R_0 = 3.2 \times 10^9\ s^{-1}$, $\omega_{HE} = 1 \times 10^7\ s^{-1}$, $\Delta_G = 1.0$ G. $t_p =$ (A) 0 ns, (B) 5 ns, (C) 10 ns, and (D) 15 ns.

underestimated. The effect of the non-ideal pulses would be improperly accounted for by slowing down the molecular motion to achieve a satisfactory fit to the experimental spectrum. However, well into the slow motional regime, where the dynamic spin packets experience large homogeneous broadening, the effects of finite pulse widths are much reduced.

3.3. Comparison with experiments

Now, we apply the arbitrary pulse 2D-ESR theory to the analysis of some experimental spectra. The system we chose was ca. 1 mM 2,2,6,6-tetramethyl-4-piperidone-*N*-oxyl-d_{15} (PD-tempone) dissolved in 85% glycerol-d_3-D_2O solvent. The reason we chose this system is that the tumbling of PD-tempone in glycerol could be simply modeled as an isotropic reorientation in an isotropic medium, and by varying the temperature we could obtain spectra ranging from fast-to-slow motion. This simple model of molecular rotation allowed us to conveniently study the effects of arbitrary pulses on 2D-ELDOR. The experiments were performed on a home-built pulsed 2D-FT ESR spectrometer described elsewhere [4,6,16].

Figs. 6 and 7 show some of the experimental 2D-ELDOR spectra of PD-tempone in 85% glycerol for different pulse widths taken over a range of temperatures. In these experimental spectra, the static magnetic field B_0 was 3280 G and the frequency was 9.2 GHz; the dead times t_{01} and t_{02} were both 50 ns; and the mixing time T_m was 100 ns. The TWT amplifier provided 1 kW output power, and a 3.2 mm ID bridged lopp gap resonator was employed. Other experimental aspects and conditions are described elsewhere [4,6,16]. To fit the spectra, we need the magnetic parameters. In a previous study [28], the magnetic hyperfine A tensor and g-tensor of PD-tempone in glycerol have been obtained from the simulations of rigid limit spectra. These magnetic parameters have been used in the theoretical simulations and have been cited above.

The model parameters used in the fits are: the isotropic rotational rate, R_0, describing the reorientation of PD-tempone in glycerol, the Gaussian inhomogeneous linewidth, Δ_G, accounting for all the line broadening other than molecular relaxation, and the Heisenberg exchange rate, ω_{HE}, to better fit the cross peaks in the 2D-ELDOR spectra, due to the magnetization transfer induced by HE during the mixing peri-

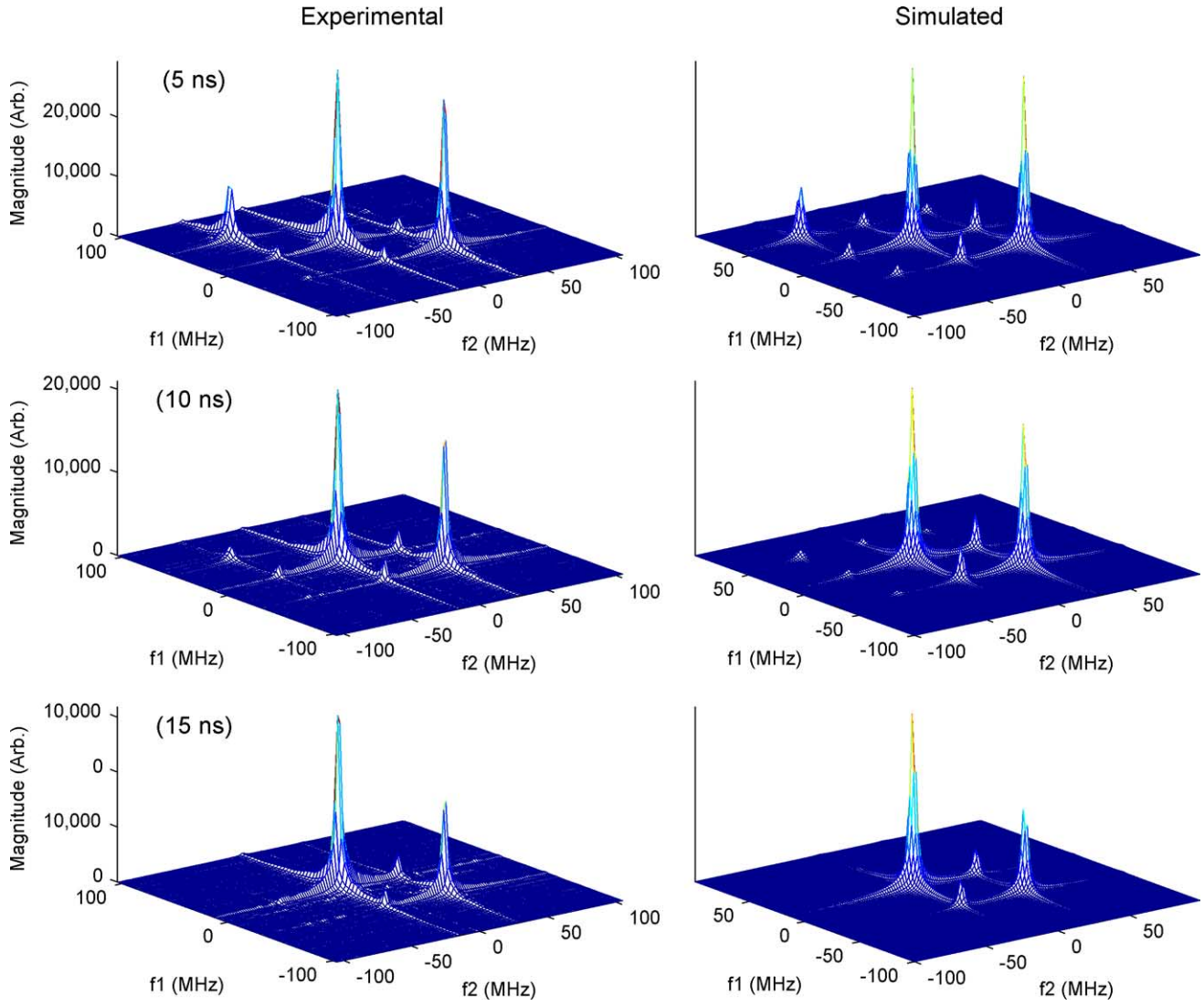

Fig. 6. Comparison of 9.2 GHz experimental (left) and simulated (right) 2D-ELDOR spectra of PD-tempone in 85% glycerol for different pulse widths at 28.7 °C. The parameters used in the simulations are given in Table 1.

od in Fig. 1. Since these parameters are independent of variations in the microwave pulse width, t_p, one could fit simultaneously the spectra of different t_p for a given temperature. In this work, however, we chose another approach. From Figs. 6 and 7, we can see that the spectra from longer pulse widths look more like slow motional spectra, i.e., they are more sensitive to the motional parameters. Therefore, for each temperature, we started from fitting the 15 ns spectrum. The fitting parameters coming out from the 15 ns fit were then used as the seed values in the fittings of the spectra of other pulse widths. Repeating this procedure a few times, we could determine finally a set of model parameters which best fit to all the spectra of different pulse widths for a given temperature. The best fit theoretical 2D-ELDOR spectra are displayed for two temperatures in Figs. 6 and 7 and the corresponding best fit model parameters are listed in Table 1 for our studies involving four different temperatures.

Table 1
Dynamic and fitting parameters

t (°C)	$R_0 \times 10^{-8}$ (s^{-1})	$\omega_{HE} \times 10^{-6}$ (s^{-1})	Δ_G (G)
28.7	11.0	3.16	0.33
14.8	3.98	2.01	0.34
11.6	3.16	1.12	0.40
7.0	1.58	0.63	0.49

The agreement between the experimental and simulated spectra is quite good, as indicated in Figs. 6 and 7 and our other results. The main spectral features of the experiment have been captured by our theory. The intensities of the outer peaks are reduced gradually as the pulse width becomes longer.

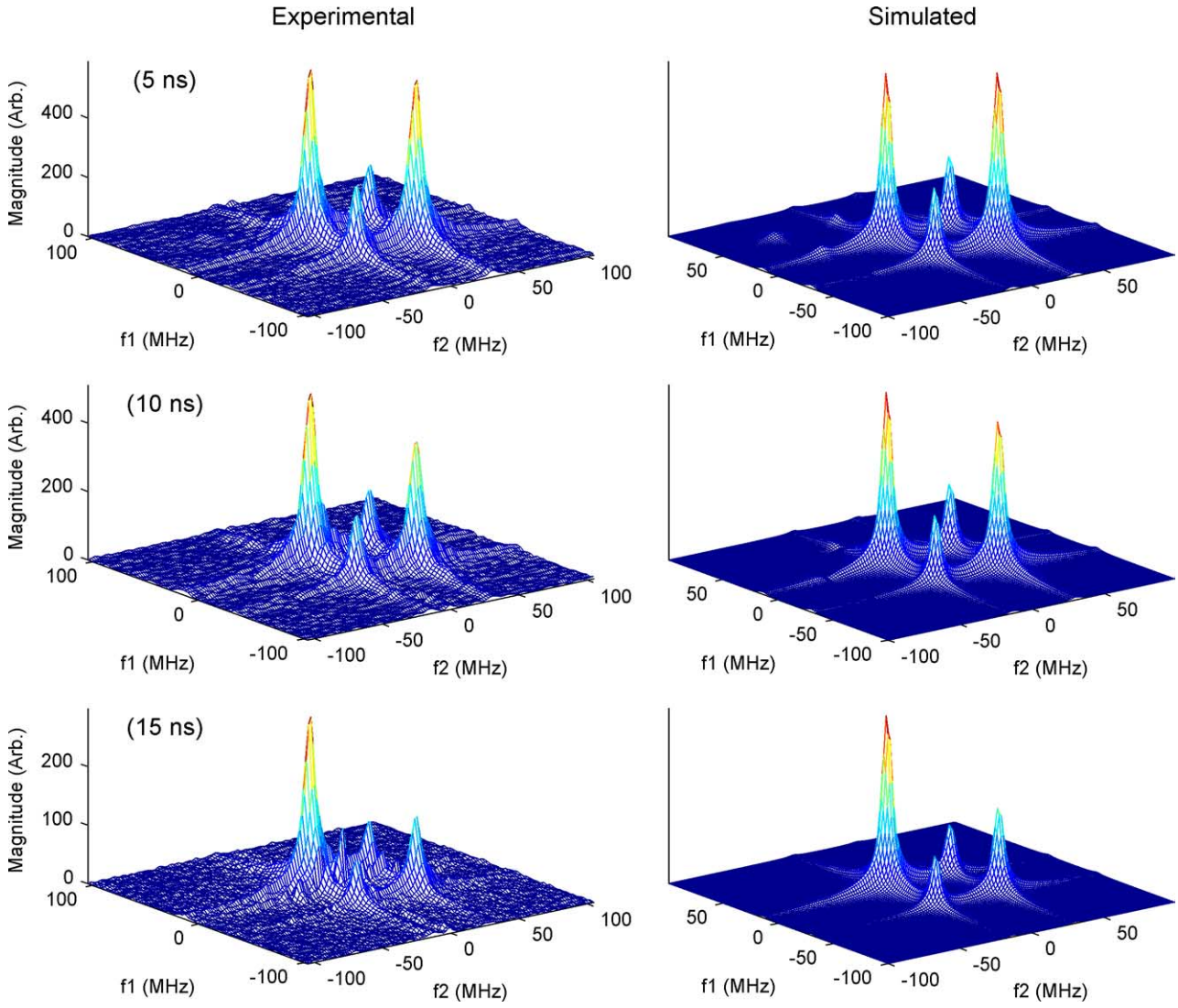

Fig. 7. Comparison of 9.2 GHz experimental (left)and simulated (right) 2D-ELDOR spectra of PD-tempone in 85% glycerol for different pulse widths at 11.6 °C. The parameters used in the simulations are given in Table 1.

3.4. Discussion

While the theory fits the experiment well and captures most experimental details, we do notice some discrepancies between the experimental and simulated spectra. Better fits may be achieved by allowing for slightly anisotropic rotational diffusion of the probe as well as a local ordering potential. In addition, a local cage might be needed [10]. Instrumental details such as the effects of the Q factor of the microwave resonator were not included in our theoretical model, although in our experiments the loaded $Q \approx 40$ was low enough not to significantly distort the pulses [6]. Also the arbitrary pulse was assumed to have a simple rectangular shape. More realistically, B_1 changes in magnitude and phase with time during the pulse (and one can measure this experimentally). In this case, the pulse propagator in Eq. (21) would be different for different Δt. This would lead to a more complicated form for the density operator $\hat{\rho}(\Omega, t_p)$ than that given in Eq. (34) for the case of a rectangular pulse, for which the operator $\hat{M}(\Omega, \Delta t)$ is simply raised the the appropriate power. Our theoretical method could readily be extended to this more general case, but it would be computationally more intensive.

Finally, we would like to note that a simple system has been chosen in this study to illustrate the effects of arbitrary pulses on 2D-ELDOR ESR spectra. The reorientation of PD-tempone in glycerol can be approximated as a spherical body rotating in an isotropic medium. For such a system, the quantum numbers L, K, and M, in the basis functions defined in Eq. (14), only need to be truncated at $L_{\max} = 6$, $K_{\max} = 4$ and $M_{\max} = 2$, respectively, to achieve the convergence. This corresponds to a matrix dimension of 60 in the off-diagonal subspace and of 93 in the diagonal subspace. However, for a system where a rod-like molecule is reorienting in an orient-

ing potential, the dimension of both the diagonal and off-diagonal matrices may be as large as a few thousand. The matrix dimensions could become much larger if the slowly relaxing local structure (SRLS) model [25,26] is needed to interpret the experimental spectra. Such large matrices would make the matrix–matrix multiplications in Eq. (34) much more time-consuming to compute. It might then be more advisable to recast the algorithm to compute Eq. (34) such that only matrix vector multiplications are used (cf. discussion, Section 3.1).

Acknowledgments

This work was supported by grants from NIH/NCCR (P41RR16292) and NSF/CHE (0098022). The computations were partly performed at the Cornell Theory Center.

References

[1] J. Gorcester, J.H. Freed, Two dimensional fourier transform ESR spectroscopy, J. Chem. Phys. 85 (1986) 5375–5377.
[2] J. Gorcester, J.H. Freed, Two-dimensional fourier transform ESR correlation spectroscopy, J. Chem. Phys. 88 (1988) 4678–4693.
[3] J. Gorcester, G.L. Millhauser, J.H. Freed, Two-dimensional electron-spin resonance, in: L. Kevan, M. Bowman (Eds.), Advances in Pulsed and Continuous Wave ESR, Wiley, New York, 1990, pp. 119–194.
[4] R.H. Crepeau, S.K. Saxena, S. Lee, B.R. Patyal, J.H. Freed, Studies of lipid membranes by two-dimensional Fourier transform ESR: enhancement of resolution to ordering and dynamics, Biophys. J. 66 (1994) 1489–1504.
[5] S. Lee, B.R. Patyal, S. Saxena, R.H. Crepeau, J.H. Freed, Two-dimensional fourier transform ESR in complex fluids, Chem. Phys. Lett. 221 (1994) 397–406.
[6] B.R. Patyal, R.H. Crepeau, J.H. Freed, Lipid-gramicidin interactions using two-dimensional Fourier-transform electron spin resonance, Biophys. J. 73 (1997) 2201–2220.
[7] A.J. Costa-Filho, Y. Shimoyama, J.H. Freed, A 2D-ELDOR study of the liquid ordered phase in multilamellar vesicle membranes, Biophys. J. 84 (2003) 2619–2633.
[8] A.J. Costa-Filho, R.H. Crepeau, P.P. Borbat, J.H. Freed, Lipid-gramicidin interactions: dynamic structure of the boundary lipid by 2D-ELDOR, Biophys. J. 84 (2003) 3364–3378.
[9] J. Gorcester, S.B. Rananavare, J.H. Freed, Two-dimensional ELDOR and ESE study of solute dynamics in smectics, J. Chem. Phys. 90 (1989) 5764–5786.
[10] V.S.S. Sastry, A. Polimeno, R.H. Crepeau, J.H. Freed, Studies of spin relaxation and molecular dynamics in liquid crystals by two dimensional fourier transform ESR: I. cholestane in butoxy benzylidene-octylaniline and dynamic cage effects, J. Chem. Phys. 105 (1996) 5753–5772.
[11] V.S.S. Sastry, A. Polimeno, R.H. Crepeau, J.H. Freed, Studies of spin relaxation and molecular dynamics in liquid crystals by two dimensional fourier transform ESR: II. PD-Tempone in butoxy benzylidene-octylaniline and dynamic cage effects, J. Chem. Phys. 105 (1996) 5773–5791.
[12] D. Xu, R.H. Crepeau, C.K. Ober, J.H. Freed, Molecular dynamics of a liquid crystalline polymer studied by two-dimensional fourier transform and cw-ESR, J. Phys. Chem. 100 (1996) 15873–15885.
[13] S. Saxena, J.H. Freed, Theory of double quantum two-dimensional electron spin resonance with applications to distance measurements, J. Chem. Phys. 107 (1997) 1317–1340.
[14] S. Lee, D.E. Budil, J.H. Freed, Theory of two-dimensional Fourier transform electron spin resonance for ordered and viscous fluids, J. Chem. Phys. 101 (1994) 5529–5558.
[15] D.E. Budil, S. Lee, S. Saxena, J.H. Freed, Non-linear least squares analysis of slow-motion EPR spectra in one and two dimensions using a modified Levenberg-Marquardt algorithm, J. Magn. Reson. 120 (1996) 155–189.
[16] P.P. Borbat, R.H. Crepeau, J.H. Freed, Multifrequency two-dimensional fourier transform ESR: an X/Ku-band spectrometer, J. Magn. Reson. 127 (1997) 155–167.
[17] W. Hofbauer, K.A. Earle, C.R. Dunnam, J.K. Moscicki, J.H. Freed, A high-power 95 GHz pulsed ESR spectrometer, Rev. Sci. Instrum. 75 (2004) 1194–1208.
[18] K.M. Salikhov, D.J. Schneider, S. Saxena, J.H. Freed, A theoretical approach to the analysis of arbitrary pulses in magnetic resonance, Chem. Phys. Lett. 262 (1996) 17–26.
[19] H.F. Trotter, On the product of semi-groups of operators, Proc. Am. Math. Soc. 10 (1959) 545–551.
[20] M. Suzuki, Decomposition of formulas of exponential operators and Lie exponentials with some applications to quantum mechanics and statistical physics, J. Math. Phys. 26 (1985) 601–612.
[21] J.H. Freed, Electron spin resonance, Ann. Rev. Phys. Chem. 23 (1972) 265–310.
[22] J.H. Freed, Theory of saturation and double resonance in ESR spectra VI: saturation recovery, J. Phys. Chem. 78 (1974) 1155–1167.
[23] D.J. Schneider, J.H. Freed, Spin relaxation and molecular dynamics, Adv. Chem. Phys. 73 (1989) 387–527.
[24] E. Meirovitch, A. Nayeem, J.H. Freed, Analysis of protein-lipid interactions based on model simulations of electron spin resonance spectra, J. Phys. Chem. 88 (1984) 3454–3465.
[25] A. Polimeno, J.H. Freed, Slow motional ESR in complex fluids: the slowly relaxing local structure model of solvent cage effects, J. Phys. Chem. 99 (1995) 10995–11006.
[26] Z. Liang, J.H. Freed, An assessment of the applicability of multifrequency ESR to study the complex dynamics of biomolecules, J. Phys. Chem. 103 (1999) 6384–6396.
[27] D.J. Schneider, J.H. Freed, Calculating slow motional magnetic resonance spectra: a user's guide, in: L.J. Berliner, J. Reuben (Eds.), Biological Magnetic Resonance, vol. 8, Plenum Publishing Corporation, New York, 1989, pp. 1–76.
[28] J.S. Hwang, R.P. Mason, L.-P. Hwang, J.H. Freed, Electron spin resonance studies of anisotropic rotational reorientation and slow tumbling in liquid and frozen media. III. Perdeuterated 2,2,6,6,-tetramethy l-4-piperidone N-oxide and an analysis of fluctuating torques, J. Phys. Chem. 79 (1975) 489–511.